Innovative catalyst integration on transparent silicone microreactors for photocatalytic applications

Ismael Pellejero (Conceptualization) (Methodology) (Investigation) (Data curation) (Writing - original draft) (Funding acquisition), Alberto Clemente (Investigation) (Data curation), Santiago Reinoso (Investigation) (Writing - review and editing), Alfonso Cornejo (Methodology) (Investigation), Alberto Navajas (Methodology) (Funding acquisition), José J. Vesperinas (Resources) (Methodology), Miguel A. Urbiztondo (Conceptualization) (Investigation) (Writing - review and editing), Luis M. Gandía (Conceptualization) (Methodology) (Supervision) (Writing - review and editing) (Funding acquisition)

PII: S0920-5861(20)30351-5

DOI: https://doi.org/10.1016/j.cattod.2020.05.058

Reference: CATTOD 12908

To appear in: *Catalysis Today*

Received Date: 7 January 2020

Revised Date: 19 April 2020

Accepted Date: 23 May 2020

Please cite this article as: Pellejero I, Clemente A, Reinoso S, Cornejo A, Navajas A, Vesperinas JJ, Urbiztondo MA, Gandía LM, Innovative catalyst integration on transparent silicone microreactors for photocatalytic applications, *Catalysis Today* (2020), doi: https://doi.org/10.1016/j.cattod.2020.05.058

Innovative catalyst integration on transparent silicone microreactors for photocatalytic applications

Ismael Pellejero[1,*], Alberto Clemente[1], Santiago Reinoso[1], Alfonso Cornejo[1], Alberto Navajas[1], José J. Vesperinas[2], Miguel A. Urbiztondo[3,*], Luis M. Gandía[1]

[1]Institute for Advanced Materials and Mathematics (InaMat[2]); Universidad Pública de Navarra (UPNA); Edificio Jerónimo de Ayanz, Campus de Arrosadia, 31006 Pamplona-Iruña, Spain.

[2]Servicio de Apoyo a la Investigación; Universidad Pública de Navarra (UPNA); Edificio El Sario, Campus de Arrosadia, 31006 Pamplona-Iruña, Spain.

[3]Centro Universitario de la Defensa; Academia General Militar, Ctra. Huesca s/n, 50090 Zaragoza, Spain.

*Corresponding Authors: ismael.pellejero@unavarra.es (I.P.), urbiz@unizar.es (M.A.U.).

Graphical Abstract:

The solid photocatalyst is dip-coated onto a 3D-printed sacrificial template made of ABS (acrylonitrile butadiene styrene) polymer, and such coated template is subsequently embedded in PDMS (polydimethylsiloxane) matrix to conform the body of the microreactor. The PDMS pre-polymer traps the photocatalyst nanoparticles while spreading across the ABS template, and once cured, this process leaves a continuous and homogeneous thin layer of photocatalytic nanoparticles intimately adhered to the microchannel polymer walls upon removal of the template with rinsing acetone.

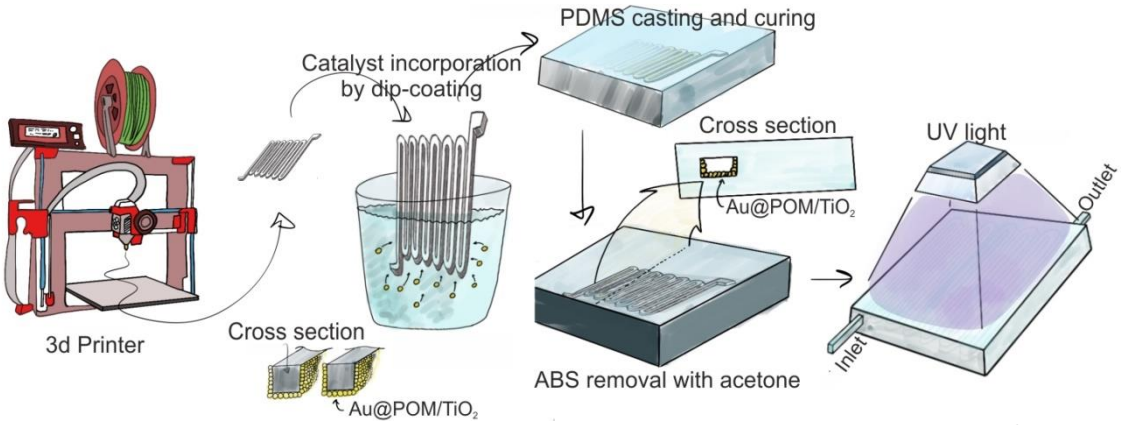

Highlights

- Innovative method for integrating Au@POM/TiO_2 nanoparticles onto silicone microreactors
- Effective adhesion of the photocatalysts to the microreactor channel walls
- Good catalytic performance of Au@POM/TiO_2 with only 0.18 % w/w. of Au nanoparticles
- Photoreduction of 4-nitrophenol performed as test reaction in continuous flow regime

Abstract

Reproducible and controllable incorporation and immobilization of catalysts and other active particles onto silicone microreactor channels is still challenging. In this work, we present an innovative fabrication protocol to attain affordable, custom-designed photocatalytic microreactors in a fast and simple manner. In this protocol, a 3D-printed ABS microreactor mold is first dip-coated with the photocatalyst, and subsequently, the catalytic layer is transferred onto the microchannel walls by indirect immobilization during the silicone casting and scaffold removal step. Serpentine-shaped microreactors have been satisfactorily fabricated with Au@POM-impregnated TiO_2 nanoparticles (Au@POM/TiO_2; Au 0.18 % w/w, POM: $H_3PW_{12}O_{40}$) as the integrated photocatalytic layer. The suitability of our fabrication method has been validated on the basis of the excellent photocatalytic performance shown by the microreactors in a model test reaction such as the continuous-flow photoreduction of 4-nitrophenol to 4-aminophenol with $NaBH_4$ and monitored by UV-Vis spectroscopy.

Keywords: 3D printing; silicone microreactors; photocatalysis; Au nanoparticles; polyoxometalates.

1 Introduction

The huge impact made by microfluidic systems during the last decade has permitted the development of a wide range of different lab-on-a-chip (LOC) devices for applications in several fields, including the biochemical, clinical, chemical and environmental areas [1-3]. Polydimethylsiloxane (PDMS) is among the most frequently used material for building microfluidic systems due to its extraordinary properties, such as biocompatibility, transparency, impermeability towards gas molecules and moisture, flexibility, or ease of replication among others [4, 5]. However, the fabrication protocol of this kind of PDMS-based devices often involves the use of sophisticated clean-room facilities and manufacture steps that are not easily

available. In particular, such microfluidic devices are usually made by soft-lithography procedures that require a mold fabricated in SU-8 resist by photolithography techniques [6].

Additive manufacturing techniques based on 3D printing constitute a prompted solution for many applications [7-10] as 3D-printing technologies enable rapid design and prototyping, while reducing costs as well as time and materials consumption. Moreover, these techniques make the development of microfluidic systems accessible to a wide range of users and allow for microfabrication at a non-specialized level. There exist many types of 3D-printing protocols [11], but that of the fused filament fabrication (FFF) is among the most popular because of its suitability even for homemade applications with very reasonable cost. The FFF technique consists in creating 3D objects following a layer-by-layer addition of a fused polymer filament under precise digital control. The resolution of this technique (minimum dimension that can be printed) depends of the nozzle diameter where plastic filament is extruded through. Standard nozzle diameters go from 800, 400, 300, to 200 μm and provide channels to similar diameter, achieving a good resolution for many applications. The ease-to-use, fast fabrication and roughly micro-scale accuracy are the main properties that makes the FFF 3D-printing protocol an ideal tool for the design and fabrication of microfluidic devices applicable in different areas [12-15] where minimum resolution is above 200 μm. In our particular case, a 3D-printed mold could enable the replacement of the SU-8 pattern [16], easily minimizing the drawbacks mentioned above. Moreover, more complex designs, that would otherwise be impossible to be created with the traditional 2D microfabrication technology, can be achieved with the FFF 3D-printing protocol.

PDMS-based microdevices are the best candidates for photocatalytic applications due to the polymer transparency in the UV-Vis spectral range [4]. Besides, these devices display several other advantages associated with the microscale performance, such as good mixing characteristics, short diffusion distances for the reactants and products and an intensified interaction between light and photocatalyst. Thus, the combination of silicone-based materials (PDMS) and 3D-printing approaches (FFF) is a promising solution to achieve functional,

affordable and customizable microfluidic photoreactors. Nonetheless, the incorporation of the photocatalyst onto the microreactor channels walls is still a challenging key step in many cases, as flushing the pristine device channels with suspensions of a given photocatalyst usually leads to poor results in terms of adhesion and homogeneity, thereby forcing the use of sophisticated surface functionalization steps. A homogeneous and adhesive distribution of the photocatalytic material is required in order to prevent any loss of such material during the reaction and to improve the effectivity overtime, and to this end, coating methods such as dip-coating or spraying are commonly used for the functionalization of PDMS surfaces due to their availability and simplicity [17, 18]. Castedo *et al*. have recently made use of a 3D-assisted procedure to fabricate parallel channel microreactors (nine rods of 500 μm width × 1 mm depth × 47 mm length) for solar hydrogen production in which the Au-doped TiO_2 photocatalyst is directly incorporated onto the internal channel surface by drop-coating prior to the microreactor sealing [19, 20]. Other researchers have in turn focused their attention on the catalyst integration during the fabrication procedure by exploring other interesting approaches including the wall surface engineering [21, 22] or the in situ incorporation by casting the polymer directly on the photocatalyst [23-25].

Another bottle-neck in the fabrication of photocatalytic microreactors is related to the fact that PDMS devices typically need to be sealed with a cover after the photocatalyst incorporation. The standard sealing must be performed by oxygen plasma bonding and this process requires flat and clean surfaces to achieve a proper sealing force, but the catalyst incorporation sometimes modifies the PDMS surface, thus making the sealing step difficult to be fulfilled or even impossible. To avoid the sealing step, different fabrication protocols based on soluble sacrificial molds like PVA (polyvinyl alcohol), wax, sugar or liquid metals have been developed [26-31]. Saggiomo and Velders [32] have established a scaffold-removal method through which a 3D-printed ABS (acrylonitrile butadiene styrene) mold is first immersed into PDMS, and lately, completely dissolved with acetone, resulting in a silicone single block that displays the desired channels without the requirement of any kind of sealing step and with the

possibility of achieving intricate and multilevel configurations. It is worth remarking that Saggiomo and Velders reported exclusively on a protocol for manufacturing pristine PDMS-based microfluidic chips, but did not describe any further procedure for the functionalization of such chips with nanoparticles or other specific coatings, which limits to great extent the applicability of the reported technique in the fabrication of functional devices such as catalytic microreactors. Therefore, we have focused our attention on developing a suitable micro-structured catalyst incorporation protocol which can entirely take place in an integrated fabrication process by combining the scaffold-removal method for fabrication with a dip-coating process for incorporation.

In this work, we have fabricated functional PDMS-based photocatalytic microreactors with the photocatalyst homogeneously distributed and firmly adhered at the silicone channel walls during curing step. Commercial TiO_2 doped with as-synthesized Au@polyoxometalate ($Au@POM/TiO_2$) nanoparticles has been selected as the photocatalyst subject to integration. The performance of the resulting microdevices has been tested in the continuous flow regime using the photoreduction of 4-Nitrophenol (4NP) to 4-Aminophenol (4AP) in the presence of $NaBH_4$ as the model reaction.

2 Materials and Methods

2.1 Preparation and characterization of the Au@POM/TiO_2 photocatalyst

The synthesis of the precursory Au@POM nanoparticles was carried out in batches by irradiating aqueous mixtures of a Au^{III}-containing starting material, an electron-mediating photoactive polyoxometalate (POM) species and a sacrificial electron donor such as propan-2-ol (IPA) with UV light. More specifically, a water solution of 0.1 mM in $HAuCl_4$ (Merck), 0.035 mM in phosphotungstic acid $H_3PW_{12}O_{40}$ (Strem) and 0.5 M in IPA (Scharlab) was deoxygenated by bubbling Ar, added to a quartz flask (20 mL) and irradiated with a 30 W Hg Lamp (Millipore S.A.S) under stirring for 25 min. The Au@POM nanoparticles contained in the

resulting pink solution were characterized by UV-Vis spectroscopy (Flame Ocean Optics spectrophotometer) and STEM (FEI Tecnai F30 transmission electron microscope at the Advanced Microscopy Laboratory-LMA at University of Zaragoza).

The Au@POM/TiO_2 photocatalyst was prepared by incipient wetness impregnation of the pre-synthesized Au@POM nanoparticles over commercial TiO_2 fabricated by flame spray pyrolysis (TECNAN Tecnología Navarra de Nanoproductos S.L; particle diameter: 20 nm to 50 nm, specific surface area: ca. 240 $m^2\ g^{-1}$). The calculated gold loading was 0.18 % w/w with respect to TiO_2. This low value of Au loading was chosen to illustrate the good photocatalytic performance of the as-synthesized Au@POM/TiO_2 nanoparticles. The structural and elemental analyses of the Au@POM/TiO_2 photocatalyst were carried out by using a scanning transmission electron microscope (STEM, FEI Tecnai F30 at the LMA) equipped with an energy dispersive spectroscopy detector (EDS).

2.2 Fabrication protocol of Au@POM/TiO_2-coated silicone microreactors

Silicone microreactors were fabricated by following the scaffold-removal procedure described by Saggiomo and Velders [32], but with some changes in order to incorporate the photocatalyst nanoparticles during the fabrication process. Fig. 1 summarizes the main steps undertaken for the fabrication of the photocatalyst-coated microreactors, which include: i) design and 3D printing of the ABS mold; ii) incorporation of the Au@POM/TiO_2 photocatalyst by dip-coating over the ABS mold; iii) PDMS casting and curing; and iv) mold removal and insertion of the microfluidic connections. Scanning electron microscopy (SEM, FEI Inspect F50) coupled to energy-dispersive X-ray spectroscopy (EDX) over samples sputtered with 20 nm of gold for a better visualization was the technique selected for characterizing and visualizing the different stages throughout the microreactor fabrication process.

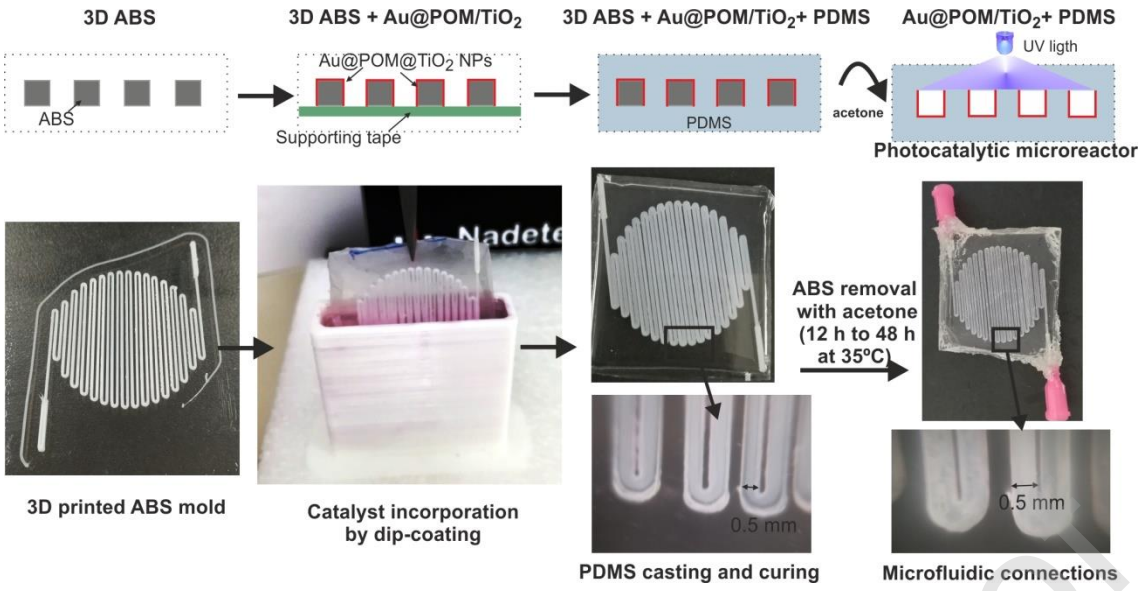

Fig. 1. Scheme of the fabrication protocol of silicone microreactors with integrated photocatalysts by following the "scaffold-removal" method.

i) Design and 3D printing of the ABS mold: a computer-aided design software (AutoCAD®) was used to design two serpentine-shaped models with squared cross-section channels of 0.5 mm × 0.5 mm (0.5 × 0.5) and 1.0 mm × 1.0 mm (1 × 1), a total estimated volume of 0.21 mL and 0.42 mL, and a theoretical length of 1070 mm and 420 mm, respectively (see supplementary Table S1 for more details on the design parameters). The sacrificial molds were fabricated in ABS (SMARTFIL® ABS Smart Materials 3D) by the fused filament fabrication technology using a replicating, rapid ZortraxM200 3D printer (extrusion parameters: nozzle 400 µm, 220 ºC, 1.75 mm filament, 10 $mm \cdot s^{-1}$).

ii) Incorporation of the $Au@POM/TiO_2$ photocatalyst by dip-coating: the deposition of the $Au@POM/TiO_2$ material over the surface of the ABS molds was carried out by dip-coating conducted with a ND-DC dip-coater system (Nadetech Innovations). A suspension of the as-synthesized photocatalyst nanoparticles was prepared by mixing $Au@POM/TiO_2$, propane-1,2-diol (Aldrich) and H_2O in a ratio 1:10:90 (w/w). Propane-1,2-diol was added to the mixture for tuning its viscosity and giving stability to the resulting suspension The mixture was then sonicated for 30 min to ensure a homogeneous dispersion. The selected 3D-printed ABS mold was first subjected to an environmental plasma treatment (corona discharge - BD-20AC

ElectroTechnic Products) for 1 min to improve its wettability, and then fixed on a scotch tape as a support for a better handling during the dip-coating process. The tape is also needed to avoid the coating of the mold top face with any photocatalyst layer, which would block the light incidence during the microreactor operation, thereby reducing its effectivity. For other potential non-photocatalytic applications, the use of this support can be avoided and the ABS mold can be dip-coated directly over all its faces. The mold was subsequently dip-coated twice into the above colloidal suspension with the following operational parameters: immersion speed 100 mm min^{-1}, waiting time 10 s, withdrawal speed 10 mm·min^{-1}. Finally, the resulting coated ABS mold was dried in an oven at 80 °C for 3 h and peeled off from the scotch tape support.

iii) PDMS casting and curing: a liquid mixture of the PDMS prepolymer (elastomer) and the curing agent (cross-linker) Sylgard 184 (Dowsil) was prepared with a ratio 10:1 (w/w) and degassed under vacuum (20 mmHg) for 30 min. The coated 3D-printed ABS mold (3D ABS + Au@POM/TiO_2) was placed inside a molding container with the aid of small PDMS pieces that are used as supports to stabilize the position of the free serpentine at the centre of the container during the subsequent PDMS pouring (see Scheme S1 in supplementary data). The molding container was then filled with the PDMS liquid mixture. After 30 additional min under vacuum followed by 30 min of curing time at 80 °C, the resulting PDMS block (3D ABS + Au@POM/TiO_2 + PDMS) was peeled off from the container and cut in square shape keeping the inlet and outlet opened.

iv) Mold removal and insertion of the microfluidic connections: the square-shaped PDMS block was immersed in acetone (Scharlab) at 35 °C for 12 to 48 h. During this period of time, the ABS mold was partially degraded and could be completely removed from the PDMS block by passing fresh acetone through the serpentine-shaped channel repeatedly until full dissolution. Possible impurities associated to acetone and rests of degraded ABS inside the channels that could poison the catalyst surface, were removed by passing propan-2-ol and later distilled water through the channel. Finally, drying was conducted by means of a dry N_2 flow and storage in an

oven at 100 °C during 1 h. Finally, connection tips (Nordson EDF) were fixed to the block inlet/outlet positions and sealed with silicone glue.

2.3 Photocatalityc test reactions

The UV-light-driven photoreduction of 4-nitrophenol (4NP) to 4-aminophenol (4AP) with $NaBH_4$ in continuous flow regime was selected as the model test reaction to evaluate the catalytic performance of the Au@POM/TiO_2-coated silicone microreactors [33]. A freshly prepared aqueous solution of 4NP (Merck, 20 mg·L^{-1}) and $NaBH_4$ (Merck, 1 g·L^{-1}) was injected into the microreactors at different volumetric flow rates (0.5, 1.0, 2.0 and 4.0 mL h^{-1}) by using a syringe pump (PHD 2000, Harvard Apparatus). A highly efficient LED (1200 mW radiant flux) was used to illuminate the microreactor at 365 ± 2 nm. The LED (LED Engin LZ1-10U600) was centred at a distance of 25 mm from the device (see supplementary Fig. S1 for more technical specifications). The irradiance was measured directly in the centre of the microreactor (4.5 mW cm^{-2}) with a BlueWave spectrometer (Stellarnet INC) before performing the experiments.

The concentration of 4NP was continuously monitored downstream in the 220-700 nm spectral range by using a UV-Vis spectrophotometer (Flame Ocean Optics) equipped with a microfluidic cell and a compact source light (DH-mini Ocean Optics). The conversion (X) of 4NP to 4AP was calculated as $X=1-A_t/A_0$ where A_t is the absorbance of 4NP at 400 nm at a given reaction time t, and A_0 is the original absorbance at $t = 0$. The presence of 4AP in samples obtained from the final reaction mixtures was confirmed by HPLC analyses, which were performed on an Agilent 1100 chromatograph coupled to an UV-Vis detector set at 245 nm (see Fig. S2 in supplementary data).

3 Results and discussion

3.1 Photocatalyst characterization

Noble metal ions such as Au^{III} are known to reduce easily to metal nanoparticles through straightforward light-driven reactions with the class of metal-oxygen anionic clusters known as polyoxometalates (POMs) acting as photocatalysts [34, 35]. Owing to the ability of undergoing fast, reversible and multi-step proton-coupled redox processes upon excitation with UV light without experiencing any substantial structural impact, the POM can simultaneously plays the roles of transferring electrons to Au^{III} from a sacrificial donor such as an alcohol (IPA in our case) and stabilizing the resulting to Au^0 nanostructure by forming an outer protective shell of clusters that prevents from further aggregation processes due to electrostatic repulsion. The results obtained from the UV-Vis and STEM characterization of the Au@POM nanoparticles synthesized in this work by UV-irradiation of a $HAuCl_4$:$H_3PW_{12}O_{40}$:IPA aqueous mixture are shown in Fig. 2. The UV-Vis spectra show the characteristic absorption band of plasmonic gold nanoparticles around 530 nm, which reaches its maximum absorbance after 25 min of irradiation time revealing the complete reduction of Au^{III} to Au^0. As illustrated in the STEM images displayed in Fig. 2 B, the shape of the Au@POM nanoparticles is nearly spherical and they show a very homogeneous size distribution. The average nanoparticle diameter was found to be 30±8 nm upon systematic measuring of the STEM images (above 100 particles).

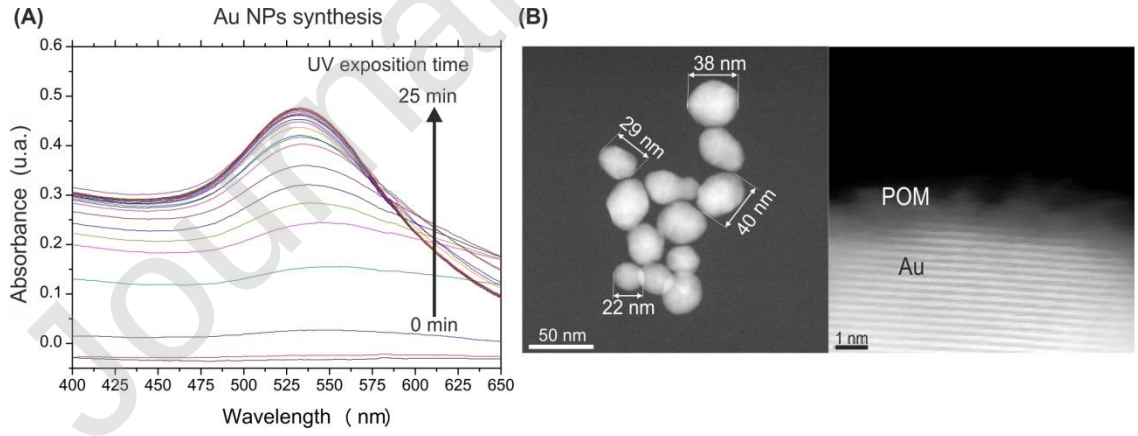

Fig. 2. Characterization of Au@POM nanoparticles: (A) UV-Vis spectra at different irradiation times; (B) STEM images of the nanoparticles at two different augmentations.

As for the TiO_2-supported catalysts, Fig. 3 depicts STEM representative images of the Au@POM/TiO_2 solid prepared by incipient wetness impregnation of commercial TiO_2 with the

Au@POM nanoparticles. These images evidence that the Au@POM nanoparticles (marked with arrows) are well dispersed on the TiO_2 matrix and do not lead to any significant agglomeration or big aggregates as expected from the low Au loading (0.18 % w/w) and the nanoparticle core-shell structure. Indeed, the protective shell of clusters of such Au@POM nanoparticles allowed for obtaining a homogeneous distribution of nanoparticle sizes during the wet impregnation of the commercial TiO_2. It is worth noting that many different POMs in terms of shape, size, composition and charge can be used for the light-driven synthesis of plasmonic metal nanoparticles suitable for integration with photoactive supports, so that the activity of the resulting photocatalytic material can be tuned by changing the nature of the POM [36]. This challenge remains open to further investigation in the near future.

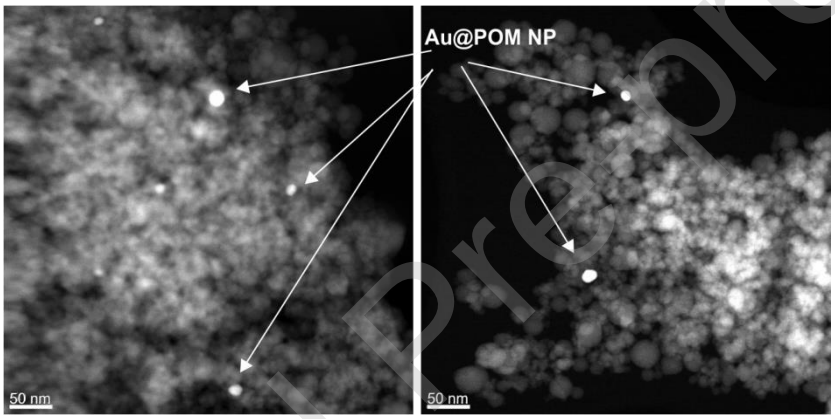

Fig. 3. STEM images of Au@POM/TiO_2 nanoparticles. The arrows highlight the places where the Au@POM nanoparticles are deposited on the TiO_2 matrix after incipient wetness impregnation.

3.2 Microreactor fabrication strategy

The strategy followed for the fabrication of the silicone microreactors is based on the scaffold-removal procedure described by Saggiomo and Velders [32], which includes as main features the design and 3D printing of a suitable mold of the microfluidic structure, the casting and curing of a silicone-based material such as PDMS, and the final degradation and removal of the sacrificial 3D printed mold. As a result, the desired microfluidic structure is fully integrated in a single block of PDMS without the need of any further sealing or bonding steps. This fact precludes any leaking problem in the resulting microdevice and facilitates the fabrication of intricate designs. The input/output tip connections are directly inserted into the microchannel

inlet and outlet positions and sealed with PDMS, which avoids any other leakage at the connections to the chip.

Direct functionalization by dip-coating of the surface of the PDMS microchannels with the selected Au@POM/TiO_2 nanoparticles results in a very fragile layer of the photocatalytic material that displays numerous cracks and very low adherence, as shown in the SEM images depicted in supplementary Fig. S3. Therefore, the novelty we propose in this work is about the simple and effective indirect integration of a solid catalytic material with a polymeric microfluidic device to construct a functional microreactor. This is accomplished by coating the 3D-printed sacrificial mold made of ABS with the solid material of interest (Au@POM/TiO_2 in our case) prior to the PDMS casting step. This fact results in a thinner and more robust layer of the Au@POM/TiO_2 photocatalyst homogeneously deposited over, and more firmly adhered to the surface of the PDMS channel walls once the latter is cured and the mold degraded and removed by the action of a solvent such as acetone.

Two serpentine-shaped Au@POM/TiO_2-coated PDMS microreactor designs (1.0 mm × 1.0 mm and 0.5 mm × 0.5 mm square-shaped sections; hereon referred to as 0.5 × 0.5 and 1 × 1, respectively) were successfully fabricated by following our modified variant of the scaffold-removal method. Dip-coating was the technique selected to cover the 3D-printed ABS molds with the as-synthesized Au@POM/TiO_2 photocatalyst because this method provides a good coverage in an easy and reliable way [37]. Two key parameters should be taken into account in order to achieve a homogenous, thin layer of the functional solid material of interest: the stabilization of the colloidal suspension of the catalyst nanoparticles and the wettability of the ABS surface, which must be suitable for the nanoparticles to graft at the sacrificial mold. An environmental plasma treatment by corona discharge was required in order to improve the wettability of the 3D-printed ABS mold, as O_2 plasma is known to enhance the hydrophilic character of the ABS surface by creating -OH groups that facilitate the adhesion of the Au@POM/TiO_2 nanoparticles [17, 38]. For both 0.5 × 0.5 and 1 × 1 microreactor designs, a suitable Au@POM/TiO_2 photocatalyst layer could be satisfactorily deposited by the dip-coating

method onto the surface of the 3D-printed sacrificial mold as confirmed by the SEM images in Fig. 4, which show a continuous and very uniform coverage all over the ABS mold. The thickness of the photocatalyst layer is estimated to range from 1.5 µm to 2 µm according to these images. The EDX analyses of such 3D ABS + Au@POM/TiO_2 systems confirmed the presence of TiO_2 grafted onto the mold surface (see Fig. S4 in supplementary data).

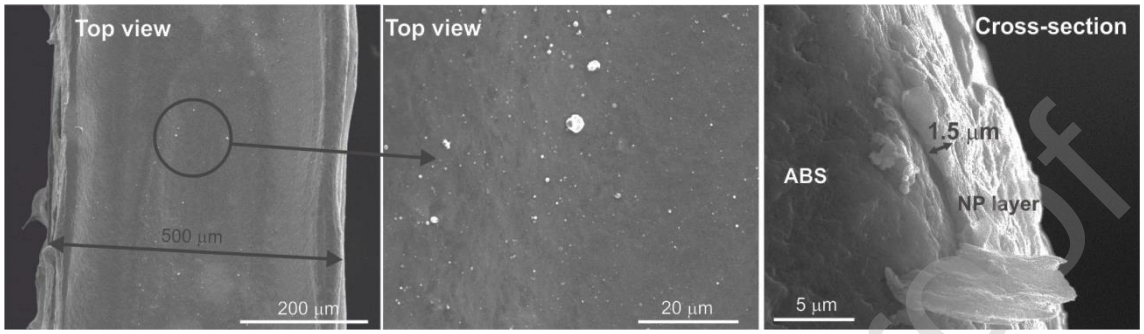

Fig. 4. SEM images at different augmentations of the 3D-printed 0.5 × 0.5 ABS mold covered with the Au@POM/TiO_2 nanoparticles upon dip-coating (3D ABS + Au@POM system). The cross-section shows the thickness of the nanoparticle coating.

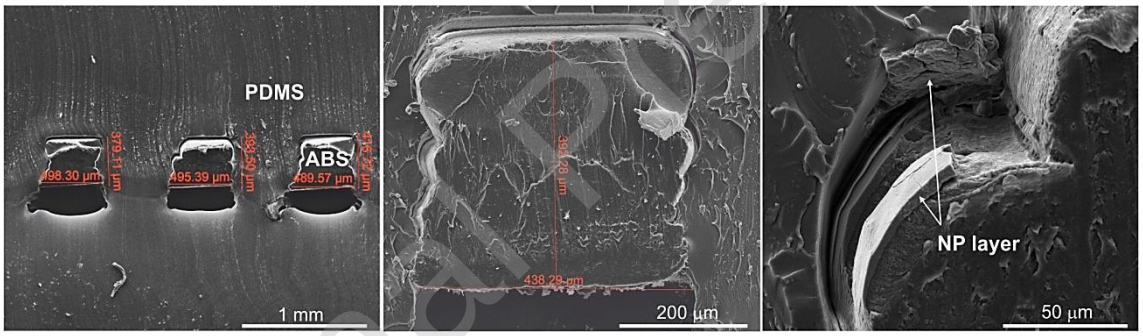

Fig. 5. SEM images at different augmentations of the cross-section of the Au@POM/TiO_2-coated, 3D-printed 0.5 × 0.5 ABS mold embedded within the PDMS block upon casting and curing (3D ABS + Au@POM/TiO_2 + PDMS system).

The cross section images of the Au@POM/TiO_2-coated 3D-printed ABS mold embedded within the PDMS block (3D ABS + Au@POM/TiO_2 + PDMS system, design 0.5 × 0.5) before the acetone dissolution step are shown in Fig. 5. A gap under the ABS mold is observed in these images as a result of the cutting process during the preparation of the sample for SEM observation. Moreover, the mold also displayed the particular cross-section originating from the fused filament addition during 3D printing. The dissolution of the ABS mold with acetone stood

out as the key fabrication step because it proved to become more difficult to fulfil as the channels are designed narrower and longer. Indeed, the 0.5 × 0.5 design presented some serious difficulties for the complete removal of the sacrificial mold due to the limited contact area and mass transfer limitations between the solvent acetone and the ABS mold inside the microchannels, thereby requiring a remarkably long dissolution time up to 48 h as a consequence (see Fig. S5 in supplementary data). On the contrary, the ABS mold could be easily degraded and removed in less than 12 h for the 1 × 1 design.

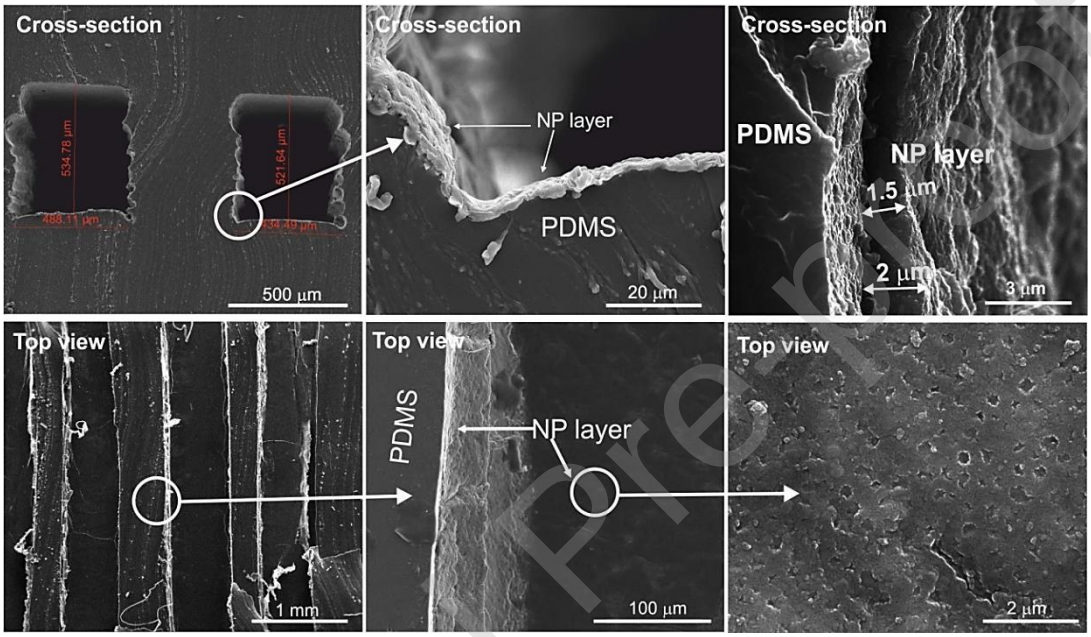

Fig. 6. SEM images of the final Au@POM/TiO_2-coated 0.5 × 0.5 PDMS microreactor upon mold removal by acetone dissolution (Au@POM/TiO_2 + PDMS system). Top: cross-section of the channels in which the photocatalyst layer has been fully transferred onto the PDMS walls. Bottom: top view of the channels showing selected nanoparticles layer.

Fig. 6 shows SEM images for the 0.5 × 0.5 design of the final Au@POM/TiO_2-coated PDMS microfluidic device (Au@POM/TiO_2 + PDMS system), which reveal the total dissolution of the sacrificial mold. The Au@POM/TiO_2 solid film remains adhered over the internal surface of the PDMS channel walls after the ABS dissolution with an estimated thickness in the 1.5 –2 µm range, which corresponds to a maximum estimated load of 12.2 mg of photocatalyst per microreactor. These results confirm the micro structured catalyst integration on the channel reactor. The homogeneous and thin photocatalyst coating is fully transferred from the ABS

mold to the PDMS block during the casting and curing steps. They also support our hypothesis about the fact that the indirect integration of the photocatalyst results in layers of the active material that show better adherence than those obtained from the direct coating over the PDMS channels (see Fig. S3 in supplementary data)

Similar fabrication results were achieved with the alternatively proposed design 1 × 1 (see Fig. S6 in supplementary data) as a complete transference of the photocatalyst layer from the ABS support to the PDMS channel walls was also observed. In this case, the ABS mold removal was faster and easier due to the larger cross-section of the channel, which facilitated solvent renewal. The maximum load was estimated at 9.6 mg of photocatalyst per microreactor. The fabrication strategy presented in this work is very simple, versatile and suitable for the development of intricate and multilayer polymeric microreactors with catalysts fully integrated at the surface of the channel walls. As a result, the firm grafting of the catalyst over the polymer matrix helps minimizing any possible leaching issue during operation. However, we have found that the complete ABS mold removal is much harder to achieve in the case of long channels (1000 mm) with a cross section shorter than 0.5 mm × 0.5 mm. In the case of intricate designs, mass transfer problems during the removal step must be taken into account when following this protocol, but they could be overcome, for example: by adding extra inlet and outlet in order to facilitate acetone accessibility or by printing an ABS scaffold with a hollow core to improve the acetone transport.

The ABS – acetone pair does not constitute the only combination possible or available for this type of scaffold-removal fabrication procedure. Many other polymeric filaments and compatible solvents can be explored, whereas stereolithography 3D printing offers a great variety of photo-curable resists and better accuracy levels. The incorporation of the catalyst to the 3D-printed mold and its later release are the key fabrication points. Dip-coating or spray-coating are simple solutions for a rapid integration of pre-formed photocatalytic solid materials, but there are lots of other possibilities to be explored in order to obtain more homogeneous coverages like CVD (chemical vapor deposition) or sputtering [39, 40].

3.3 Photocatalytic performance

The photoreduction of 4NP to 4AP in the presence of an excess of $NaBH_4$ as the reducing agent was selected as the model reaction for assessing the photocatalytic performance of the Au@POM/TiO_2-coated PDMS microreactors [41, 42]. This reaction is catalyzed by Au nanoparticles and results easy to monitor by UV-Vis spectroscopy, thereby becoming certainly useful to compare the performance of different microreactors and to address a satisfactory and homogeneous distribution of the photocatalyst onto the channel walls. Scheme 1 depicts the mechanistic model for the reduction of 4NP to 4AP catalyzed by gold in the presence of $NaBH_4$. The Au@POM nanoparticles act as electron scavengers of the electron-hole pair generated in the photocatalyst (TiO_2) upon UV light irradiation. It has been reported that POM shell has an important role as electron shuttle promoting the electron exchange on the catalyst surface [43], thus enhancing the photocatalytic performance of Au@POM NP in comparison to bare Au structures [44]. The $NaBH_4$ is decomposed by hydrolysis to generate hydrogen that is promoted to and adsorbed at the electron rich surface of the Au@POM nanoparticles. Finally, the hydrogen at the surface reacts with 4NP to yield the product 4AP.

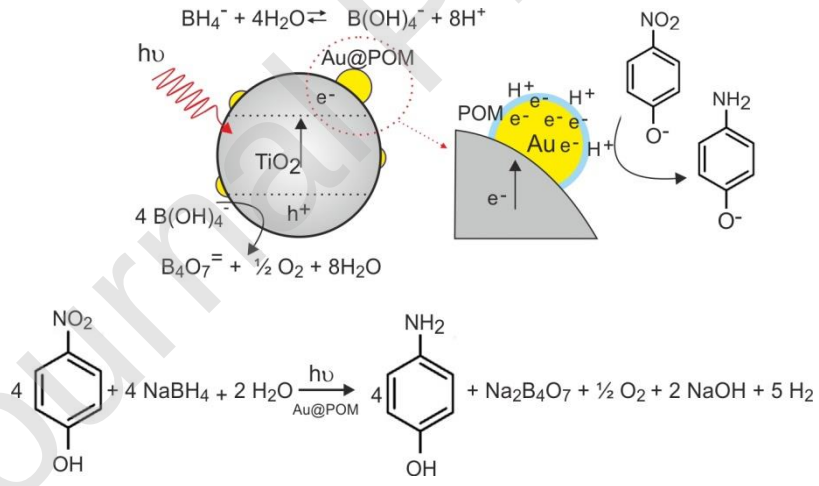

Scheme 1. Mechanistic model for the photoreduction of 4NP to 4AP catalyzed by Au@POM/TiO_2 coating.

The pristine 4NP and the photoproduct 4AP present characteristic absorption maxima in basic solution at ca. 400 and 300 nm, respectively. Monitoring these two absorbance bands facilitates calculating the yield of the photoreaction. Several microreactors of the two different

designs developed in this work (0.5 × 0.5 and 1 × 1) were tested at different total flow rates ranging from 0.5 to 4.0 mL h^{-1}.

This reaction is very sensitive to the presence of metal nanoparticles [41, 42] according to preliminary experiments we performed in batch mode. From these experiments, we could determine that, when the content of Au@POM nanoparticles reached 1 % w/w, the reaction afforded similar yields regardless of whether it was carried out with or without light. Thus, we selected a low Au loading as low as 0.18 % w/w to be able to differentiate the activity of the microreactors between light and dark conditions and to characterize them for photocatalytic applications.

A series of experiments was conducted to evaluate the activity of the photocatalyst with three different microreactors (1 × 1 design): a blank microreactor without any photocatalyst deposited at the surface of the bare PDMS channels, one microreactor coated with the commercial TiO_2 support and another microreactor coated with the Au@POM/TiO_2 photocatalyst prepared in this work (Au 0.18 % w/w). Fig. 7 depicts the UV-Vis spectra obtained from such microreactors after reaching the steady state at a flow rate of 2 mL h^{-1} and compared with the spectrum of a pristine 4NP aqueous solution. The bare PDMS microreactor tested under UV light allowed for the photodegradation of 4NP by sensitization of the dye as indicated by the decay of the intensity of absorption maximum at 400 nm, but the lack of any absorbance at 300 nm together with the observation of the characteristic band of phenol at 270 nm confirmed that the 4NP substrate could not be photoreduced to 4AP under these conditions. The TiO_2-coated microreactor showed photodegradation to some extent, as a decrease in the intensity of the 4NP band at 400 nm occurred along with a slight increase in that at 300 nm associated with the photoproduct 4AP. This fact is attributed to the intrinsic photocatalytic properties of titania. Finally, the absorbance at 400 nm becomes very weak for the microreactor coated with the Au@POM/TiO_2 photocatalyst, and results in a high 4NP conversion of around 93 % and a removal of 27.8 μmol · h^{-1} · g(cat.)$^{-1}$. The photoreduction of 4NP is heavily dependent on the presence of Au nanoparticles, which promote electron transfer

from the TiO_2 to the 4NP molecules adsorbed on them [45]. HPLC-UV-Vis analysis of 4AP containing mixtures is challenging as 4AP is an ampholite and thus its analysis requires careful control of the pH in the mobile phase as well as the absorption wavelength; hence UV-Vis spectroscopy is commonly accepted as routine analytical technique for monitoring this reaction. In our case the reaction mixtures were qualitatively analyzed by HPLC (see supplementary Fig. S2) in order to unambiguously confirm the presence of 4AP in the reaction mixture, prior to routine UV-Vis quantification.

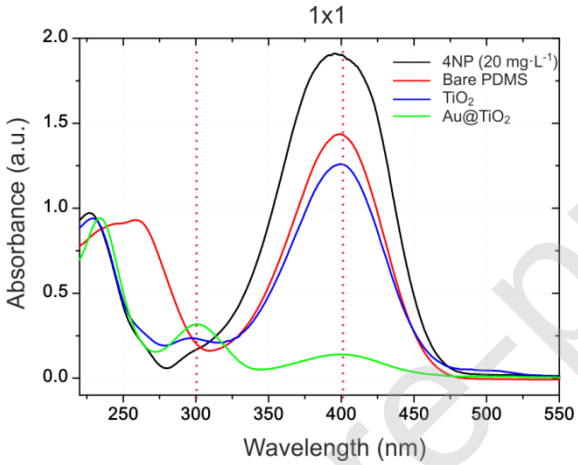

Fig. 7. UV–Vis spectra at steady state for the photoreduction of 4NP in three different 1 × 1 microreactors: bare PDMS, TiO_2-coated PDMS, and Au@POM/TiO_2-coated PDMS (flow rate 2 mL·h^{-1}, t_r = 12.5 min).

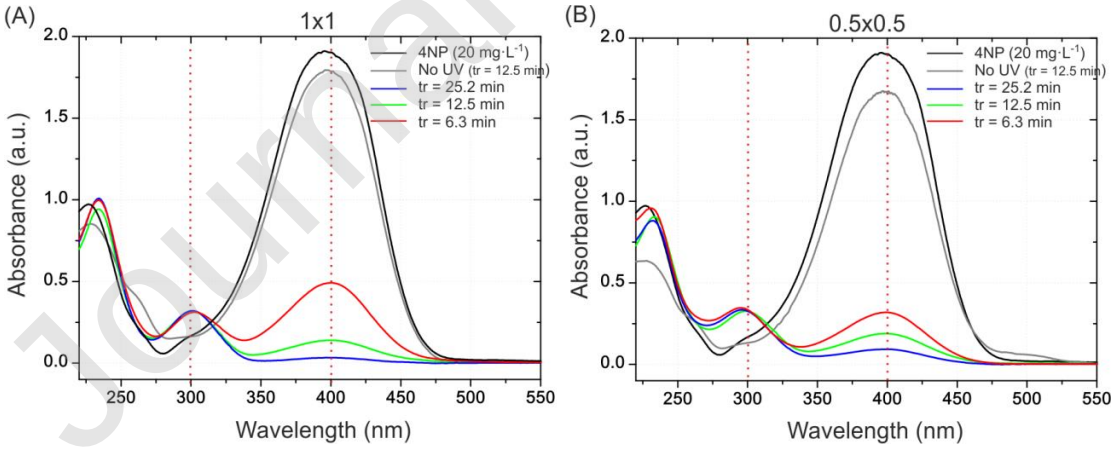

Fig. 8. UV–Vis spectra for the photoreduction of 4NP in Au@POM/TiO_2-coated PDMS: (A) design 1 × 1 at flow rates 1, 2 and 4 mL h^{-1} (t_r = 25.2, 12.5 and 6.3 min), and (B) design 0.5 × 0.5 at flow rates 0.5, 1 and 2 mL h^{-1} (t_r = 25.2, 12.5 and 6.3 min). The spectra were recorded at a reaction time of 60 min.

Two Au@POM/TiO_2-coated microreactors of both designs were selected to carry out the photoreduction of 4NP at different flow rates (see Fig. 8). The 4NP conversions achieved at residence times (t_r) of 6.3, 12.5 and 25.2 min (flow rates of 1, 2 and 4 mL h^{-1}) were 75, 93 and 98 % for the 1 × 1 microreactor and 83, 90 and 95 % for the 0.5 × 0.5 microreactor, respectively. Blank experiments without any UV-light irradiation carried out at t_r = 12.5 min in both systems gave low 4NP conversions of 6 and 12 % for the 1 × 1 and 0.5 × 0.5 designs, respectively. In absence of any incident UV light, the higher conversion provided by the microreactor with the shorter cross-section dimensions (0.5 × 0.5) can be attributed to its higher surface-to-volume ratio and higher photocatalyst load, and therefore, to an improved contact of 4NP with the Au@POM/TiO_2 catalyst. Under UV-light irradiation, both microreactors displayed very good photocatalytic performances even for the shortest residence times, affording conversions higher than 90 % for t_r = 12.5 and 25.2 min. This observation demonstrates the good transference and integration of the photocatalyst during fabrication, as well as its homogeneous distribution inside the microrreactor channels. Comparing both designs, the 0.5 × 0.5 microreactor displayed better performance at t_r = 6.3 min due to its higher photocatalyst load and larger surface-to-volume ratio, as mentioned above. On the contrary, our results showed that the performance of the 1 × 1 microreactor with lower photocatalyst load became slightly better than that of the 0.5 × 0.5 design when t_r = 12.5 and 25.2 min. This fact could be related to the photocatalyst being more accessible to light than that in the 0.5 × 0.5 microreactor, in which photons can get blocked more easily by the PDMS walls due to the shortest cross-section of the microchannels.

Semiconducting oxides doped with metallic nanoparticles, especially Au and Ag, have been extensively studied for the photoreduction of 4NP to 4AP in batch slurry reactors [46-51]. All of these materials with typical dopant loads equal to or higher than 1 % have shown good catalytic performances, reaching conversions higher than 90 % in less than 30 min. Our Au@POM/TiO_2 catalyst shows comparable results in terms of conversion, but with the reaction carried out in continuous flow mode, with a much lower load of the dopant (0.18 % w/w of Au@POM,

around five times lower), and without the need of separating the catalyst. These facts highlight the advantages of the photocatalytic microreactor systems designed and manufactured in this work. Moreover, the plasmon resonance of Au@POM makes this photocatalyst suitable to carry out reactions not only under UV but also under visible light [52]. Anyway, the plasmonic metal content would have to be increased in order to achieve significant photocatalytic activities.

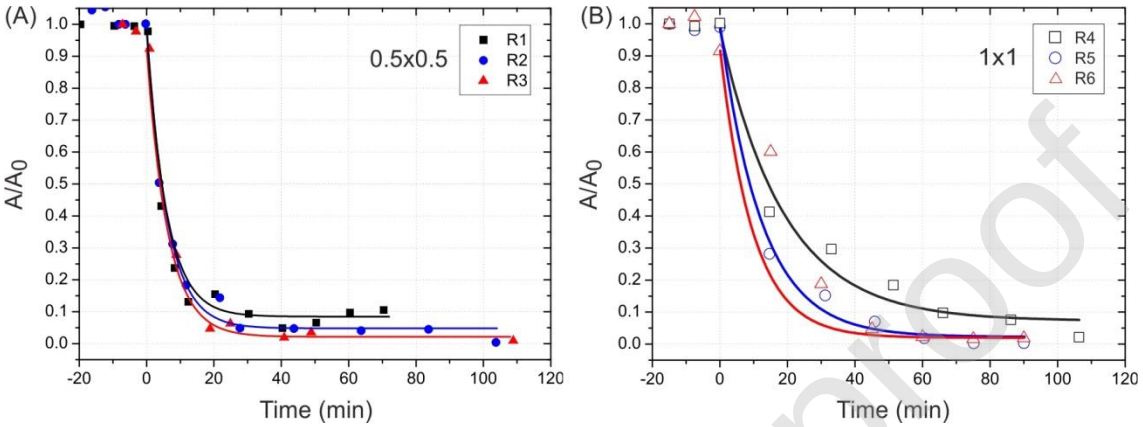

Fig. 9. UV–Vis absorbance at 400 nm vs. reaction time for the photoreduction of 4NP in six PDMS + Au@POM/TiO₂ microreactors. (A) R1−R3; dimensions 0.5 mm × 0.5 mm and (B) R4-R6; dimensions 1 mm × 1 mm). Residence time of 25.2 min.

Finally, Fig. 9 depicts the evolution under transitory regime of the quotient (A/A_0) between the absorbance at 400 nm at a flow rate of 0.5 mL h^{-1} (t_r = 25.2 min) to assess the performance of three 0.5 × 0.5 microreactors (labelled as R1–R3) and three 1 × 1 microreactors (labelled as R4–R6). At t = 0 min, the UV light source was switched on and the absorbance was registered in the optic cell placed downstream. After a period of c.a. 30 min the microreactors had reached reasonable stable response and noticeable catalytic performances, giving rise to 4NP conversions higher than 90 % for 0.5 × 0.5 that remained stable. The 1 × 1 reactors achieved conversions up to 98% but, the stability was worse. As discussed before, the microfluidic behavior is better in narrow channels leading to a stable performance, but light is more accessible in wider channels resulting in higher conversions.

From the fabrication viewpoint, both designs, 1 x 1 and 0.5 × 0.5 microreactors were satisfactorily manufactured with comparable coating morphologies and afforded reproducible

results in the selected model test reaction. However, ABS removal step with acetone is critic in the case of narrower channels and long reactors such us 0.5 × 0.5 design and must be conducted under more strict conditions. A compromise between channel diameter and reactor length must be taken into account in order to facilitate dissolution. Making use of higher temperatures during the acetone dissolution step or ABS scaffolds with hollow cores could improve the mass transfer and facilitate the fabrication. Hence, such design and fabrication method could be envisioned for being implemented in *e.g.* waste-water treatment systems.

4 Conclusions

A new approach for integrating solid catalysts with polymer-based microreactors has been successfully developed and tested for photocatalytic applications in this work. The microfabrication protocol is based on the known 3D-printed scaffold–removal method, but involves the incorporation of photocatalyst nanoparticles at the surface of an ABS mold prior to the polymer casting and mold dissolution steps, which is satisfactorily achieved just by dip-coating. To this end, plasma pre-treatment has been found to be essential in order to modulate the wettability of the ABS substrate. The transference of the nanoparticles from the surface of the ABS mold to the PDMS matrix takes place during the curing step, and is followed by the mold removal throughout a dissolution process with acetone. As a result, a PDMS block with the channel walls coated with a firmly adhered homogeneous thin layer (< 2 μm) of the catalyst of interest is obtained. The dissolution of the ABS mold has been found to be a critical step of the process, especially in the case of narrower and long channels which requires long time and superior temperature of the acetone bath.

Several microreactors coated with Au@POM/TiO_2 nanoparticles (0.18 % w/w of Au; POM: $H_3PW_{12}O_{40}$) as the photocatalytic active layer were evaluated in the UV-light-driven reduction of 4-nitrophenol to 4-aminophenol with $NaBH_4$, showing excellent photoactivity of the Au@POM nanoparticles used as co-catalyst. The conversions achieved were higher than 90 % at residence times longer than t_r = 12.5 min for both serpentine microrreactor designs tested as monitored by UV-Vis spectroscopy, highlighting the good distribution of the photocatalyst all

over the channels achieved with this method. We have been able to identify the 1 mm × 1 mm serpentine microreactor with easier and cheaper manufacturing and operability than narrower one could be implemented for waste-water treatment.

In summary, this study provides an innovative, simple and effective approach for integrating functional solid nanomaterials with polymeric microfluidic devices, which may offer new applications not only in heterogeneous catalysis or photochemistry as illustrated in the present work, but also in several other different fields such as nanocomposites or antibacterial surfaces depending on the functionality of the selected nanoparticles.

Author statement

Ismael Pellejero: Conceptualization, Methodology, Investigation, Data Curation, Writing - Original Draft, Funding acquisition. **Alberto Clemente:** Investigation, Data Curation, **Santiago Reinoso**: Investigation, Writing - Review & Editing. **Alfonso Cornejo**: Methodology, Investigation. **Alberto Navajas**: Methodology, Funding acquisition. **José J. Vesperinas:** Resources, Methodology. **Miguel A. Urbiztondo**: Conceptualization, Investigation, Writing - Review & Editing. **Luis M. Gandía:** Conceptualization, Methodology, Supervision, Writing - Review & Editing, Funding acquisition.

Declaration of interests

The authors declare that they have no known competing financial interests or personal relationships that could have appeared to influence the work reported in this paper.

Acknowledgments

Financial support from Gobierno de Navarra (grants PC025-26 and PI030) and Spanish Ministerio de Ciencia, Innovación y Universidades, and the European Regional Development Fund (ERDF/FEDER) (grant RTI2018-096294-B-C31) is gratefully acknowledged. I. P. and S. R. thank Obra Social la Caixa, Fundación Caja Navarra and Universidad Pública de Navarra (UPNA) for their research contracts in the framework of the programs “Ayudas Postdoctorales”

and “Captación del Talento”. L.M.G. thanks Banco de Santander and UPNA for their financial support under "Programa de Intensificación de la Investigación 2018" initiative. Centro Tecnológico Lurederra is gratefully acknowledged for its partnership in the project FOREST (PC025-026). The microscopy works have been conducted in the "Laboratorio de Microscopias Avanzadas" at "Instituto de Nanociencia de Aragon - Universidad de Zaragoza". Authors acknowledge the LMA-INA for offering access to their instruments and expertise.

References

[1] S. Haeberle, R. Zengerle, Lab Chip 7 (2007) 1094-1110.

[2] D. Heggo, S. Ookawara, Chem. Eng. Sci. 169 (2017) 67-77.

[3] C.D. Chin, V. Linder, S.K. Sia, Lab Chip 7 (2007) 41-57.

[4] J.C. McDonald, G.M. Whitesides, Acc. Chem. Res. 35 (2002) 491-499.

[5] D.C. Duffy, J.C. McDonald, O.J.A. Schueller, G.M. Whitesides, Anal. Chem. 70 (1998) 4974-4984.

[6] J.C. McDonald, D.C. Duffy, J.R. Anderson, D.T. Chiu, H. Wu, O.J.A. Schueller, G.M. Whitesides, Electrophoresis 21 (2000) 27-40.

[7] G.W. Bishop, J.E. Satterwhite-Warden, K. Kadimisetty, J.F. Rusling, Nanotechnology 27 (2016) 284002.

[8] A.A. Yazdi, A. Popma, W. Wong, T. Nguyen, Y. Pan, J. Xu, Microfluid. Nanofluid. 20 (2016) 50.

[9] N. Bhattacharjee, A. Urrios, S. Kang, A. Folch, Lab Chip 16 (2016) 1720-1742.

[10] R. Amin, S. Knowlton, A. Hart, B. Yenilmez, F. Ghaderinezhad, S. Katebifar, M. Messina, A. Khademhosseini, S. Tasoglu, Biofabrication 8 (2016) 022001.

[11] C. Parra-Cabrera, C. Achille, S. Kuhn, R. Ameloot, Chem. Soc. Rev. 47 (2018) 209-230.

[12] A.J.L. Morgan, L. Hidalgo San Jose, W.D. Jamieson, J.M. Wymant, B. Song, P. Stephens, D.A. Barrow, O.K. Castell, PLoS One 11 (2016) e0152023.

[13] A.M. Tothill, M. Partridge, S.W. James, R.P. Tatam, J. Micromech. Microeng. 27 (2017) 035018.

[14] I. Zein, D.W. Hutmacher, K.C. Tan, S.H. Teoh, Biomaterials 23 (2002) 1169-1185.

[15] F. Ning, W. Cong, J. Qiu, J. Wei, S. Wang, Compos. Part B Eng. 80 (2015) 369-378.

[16] G. Comina, A. Suska, D. Filippini, Lab Chip 14 (2014) 424-430.

[17] M. Watanabe, Soft Matter 8 (2012) 1563-1569.

[18] A.R. Madaria, A. Kumar, C. Zhou, Nanotechnology 22 (2011) 245201.

[19] A. Castedo, E. Mendoza, I. Angurell, J. Llorca, Catal. Today 273 (2016) 106-111.

[20] A. Castedo, I. Uriz, L. Soler, L.M. Gandía, J. Llorca, Appl. Catal. B Environ. 203 (2017) 210-217.

[21] S.M. Kim, Y.H. Park, S.W. Seo, C.P. Park, S.Y. Park, I. In, Adv. Mater. Interfaces 2 (2015) 1500174.

[22] I. Wong, C.-M. Ho, Microfluid. Nanofluid. 7 (2009) 291.

[23] D.S. De Sá, B.A. Marinkovic, E.C. Romani, T. Del Rosso, R.O.M.A. de Souza, A. Massi, O. Pandoli, J. Flow Chem. 6 (2016) 101-109.

[24] G.T. Roman, T. Hlaus, K.J. Bass, T.G. Seelhammer, C.T. Culbertson, Anal. Chem. 77 (2005) 1414-1422.

[25] R. Chen, L. Li, X. Zhu, H. Wang, Q. Liao, M.-X. Zhang, Energy 83 (2015) 797-804.

[26] L.M. Bellan, E.A. Strychalski, H.G. Craighead, J. Vac. Sci. Technol. B 26 (2008) 1728-1731.

[27] W.H. Goh, M. Hashimoto, Macromol. Mater. Eng. 303 (2018) 1700484.

[28] Z. Li, J. Yang, K. Li, L. Zhu, W. Tang, RSC Adv. 7 (2017) 3313-3320.

[29] Y. He, J. Qiu, J. Fu, J. Zhang, Y. Ren, A. Liu, Microfluid. Nanofluid. 19 (2015) 447-456.

[30] L. Zhou, G. Zhuang, G. Li, Sens. Actuators B Chem. 261 (2018) 364-371.

[31] D.P. Parekh, C. Ladd, L. Panich, K. Moussa, M.D. Dickey, Lab Chip 16 (2016) 1812-1820.

[32] V. Saggiomo, A.H. Velders, Adv. Sci. 2 (2015) 1500125.

[33] L. Zhang, Z. Liu, Y. Wang, R. Xie, X.-J. Ju, W. Wang, L.-G. Lin, L.-Y. Chu, Chem. Eng. J. 309 (2017) 691-699.

[34] S. Mandal, P. Selvakannan, R. Pasricha, M. Sastry, J. Am. Chem. Soc. 125 (2003) 8440-8441.

[35] A. Troupis, A. Hiskia, E. Papaconstantinou, Angew. Chem.-Int. Ed. 41 (2002) 1911-1914.

[36] U. Jameel, M. Zhu, X. Chen, Z. Tong, J. Mater. Sci. 51 (2016) 2181-2198.

[37] J.-H. Yang, Y.-S. Han, J.-H. Choy, Thin Solid Films 495 (2006) 266-271.

[38] M. Lafuente, E. Martínez, I. Pellejero, M.C. Artal, M.P. Pina, Plasma Process. Polym. 14 (2017) e1700019.

[39] D. Rafieian, R.T. Driessen, W. Ogieglo, R.G.H. Lammertink, ACS Appl. Mater. Interfaces 7 (2015) 8727-8732.

[40] R.S. Pessoa, V.P. dos Santos, S.B. Cardoso, A.C.O.C. Doria, F.R. Figueira, B.V.M. Rodrigues, G.E. Testoni, M.A. Fraga, F.R. Marciano, A.O. Lobo, H.S. Maciel, Appl. Surf. Sci. 422 (2017) 73-84.

[41] P. Zhao, X. Feng, D. Huang, G. Yang, D. Astruc, Coord. Chem. Rev. 287 (2015) 114-136.

[42] A.M. Khalil, V. Georgiadou, M. Guerrouache, S. Mahouche-Chergui, C. Dendrinou-Samara, M.M. Chehimi, B. Carbonnier, Polymer 77 (2015) 218-226.

[43] H. Park, W. Choi, Catal. Today 101 (2005) 291-297.

[44] R.R. Ozer, J.L. Ferry, Environ. Sci. Technol. 35 (2001) 3242-3246.

[45] S. Sarina, E.R. Waclawik, H. Zhu, Green Chem. 15 (2013) 1814-1833.

[46] A. Hernandez-Gordillo, V.R. Gonzalez, Chem. Eng. J. 261 (2015) 53-59.

[47] M.M. Mohamed, M.S. Al-Sharif, Appl. Catal. B-Environ. 142 (2013) 432-441.

[48] Z.W. Seh, S.H. Liu, S.Y. Zhang, K.W. Shah, M.Y. Han, Chem. Commun. 47 (2011) 6689-6691.

[49] S. Cipagauta-Díaz, A. Estrella-González, R. Gómez, Mat. Sci. Semicon. Proc. 89 (2019) 201-211.

[50] Z.-H. Ren, H.-T. Li, Q. Gao, H. Wang, B. Han, K.-S. Xia, C.-G. Zhou, Mater. Des. 121 (2017) 167-175.

[51] J.S. Wu, J.S. Wang, T.N. Wang, L.M. Sun, Y.C. Du, Y.L. Li, H.Y. Li, Appl. Surf. Sci. 466 (2019) 342-351.

[52] J. Graus, C.J. Bueno-Alejo, J.L. Hueso, Catalysts 8 (2018) 354.